Journal of Computational Design and Engineering, 2022, **10**, 108–121

DOI: 10.1093/jcde/qwac132
Advance access publication date: 15 December 2022
Research Article

Wind turbine maximum power point tracking control based on unsupervised neural networks

Eduardo Muñoz-Palomeque [1,*], J. Enrique Sierra-García [1] and Matilde Santos [2]

[1]Department of Electromechanical Engineering, University of Burgos, Burgos, 09006, Spain
[2]Institute of Knowledge Technology, Complutense University of Madrid, Madrid, Spain
*Corresponding author. E-mail: edugmunozp@gmail.com

Abstract

The main control goal of a wind turbine (WT) is to produce the maximum energy in any operating region. When the wind speed is under its rated value, the control must aim at tracking the maximum power point of the best power curve for a specific WT. This is challenging due to the non-linear characteristics of the system and the environmental disturbances it is subjected to. Direct speed control (DSC) is one of the main techniques applied to address this problem. In this strategy, it is necessary to design a speed controller to adjust the generator torque so to follow the optimum generator speed. In this work, we improve the DSC by implementing this speed controller with a radial basis function neural network (NN). An unsupervised learning algorithm is designed to tune the weights of the NN so it learns the control law that minimizes the generator speed error. With this proposed unsupervised neural control methodology, the electromagnetic torque that allows the optimal power extraction is obtained, and thus the best power coefficient (C_p) values. The proposal is tested on the OpenFAST non-linear model of the National Renewable Energy Laboratory 1.5 MW WT. Simulation results prove the good performance of this neuro-control approach as it maintains the WT variables into the appropriate range and tracks the rated operation values. It has been compared with the controller included in OpenFAST giving up to 7.87% more power.

Keywords: wind turbine, MPPT, radial basis function neural network, direct speed control

1. Introduction

The growing interest in renewable energies in recent decades has made them become a topic of constant research. With the intention of reducing the use of fossil fuels, special attention is being paid to improving clean alternative technologies. With them, the increase in efficiency in energy production is a closer reality, as well as the reduction of the environmental impact and the effect on climate change. In this line, wind power generators are one of the most used resources (Tiwari & Babu, 2016), together with solar photovoltaic energy (Hernández & Santos, 2021; Saxena *et al.*, 2020; Saxena *et al.*, 2021a) and other clean sources (Lobo & Santos, 2019; Zhou *et al.*, 2020).

Wind energy devices demand increasingly accurate and sophisticated electronic systems, more advanced generators, and efficient control to strengthen the robustness of the solutions and to improve energy production (Hossain & Ali, 2022; Tomás-Rodríguez & Santos, 2019). Thus, wind turbines (WTs) are in continuous development, in which the optimization of the operation is a key issue.

In this context, control plays an important role in wind power. Depending on the region of operation of the wind device and environmental conditions, various control actions can be applied. For example, the pitch angle of the blades, the angular speed of the generator, or the yaw angle of the nacelle can be adjusted. In all cases, the ultimate goal of the control is to make the most of the wind resource to produce more energy. The pitch angle control is used to modify the area of the blades facing the wind to stabilize the WT around its nominal power when the wind speed exceeds its rated value. On the other hand, the angular speed of the rotor is controlled to follow the best power curve for a specific WT, which is usually called maximum power point tracking (MPPT), and is applied in the region of operation of the turbine when the wind is below its rated value. The MPPT control concept is also applied in the solar energy field (Saxena *et al.*, 2021b). Finally, the yaw control rotates the nacelle to match the wind direction (Horno *et al.*, 2020).

In this work, we have focused on MPPT control. The challenges of this control are fundamentally due to the non-linearity of the WT and to the fact that it may be subjected to environmental disturbances, especially to changes in climate conditions that also present uncertainty. One of the most used control techniques in this WT region is direct speed control (DSC; Abad *et al.*, 2011). This control strategy calculates the generator speed reference based on the optimum power coefficient; then, considering the speed error, it adjusts the generator torque by means of a regulator, usually a proportional-integral-derivative (PID) controller. Since the relationship between speed error and torque is not linear and it depends on the operating point, the use of a PID for this task has some limitations (Zouggar *et al.*, 2021). To reduce the influence of the operating point, a gain-scheduling strategy can be implemented; however, this complicates the tuning of the controller in real time. For this reason, research has been carried out on the application of intelligent control techniques that have given good results for this and other WT control problems (Hemanth Kumar

Received: July 29, 2022. **Revised:** November 13, 2022. **Accepted:** December 13, 2022
© The Author(s) 2022. Published by Oxford University Press on behalf of the Society for Computational Design and Engineering. This is an Open Access article distributed under the terms of the Creative Commons Attribution-NonCommercial License (https://creativecommons.org/licenses/by-nc/4.0/), which permits non-commercial re-use, distribution, and reproduction in any medium, provided the original work is properly cited. For commercial re-use, please contact journals.permissions@oup.com

Downloaded from https://academic.oup.com/jcde/article/10/1/108/6912246 by guest on 07 July 2024

et al., 2018; Pande *et al.*, 2021; Sierra-García & Santos, 2021b; Sierra-Garcia & Santos, 2022).

In this sense, neural networks (NNs) have been successfully applied to model and control complex systems, including WTs, as they are able to adapt to changes in the environment and learn the best control law for a system (Sierra-García & Santos, 2021a). For this reason, in this work it is proposed to replace the PID regulator in the DSC strategy with an NN capable of learning online to control a land-based WT through the MPPT. The NN implements the control law and its adaptability is achieved through an unsupervised learning algorithm (ULA) that iteratively adjusts the weights of the NN to reduce the error. This characteristic allows it to adapt to changes in the system, to deal with uncertainties, and to work correctly in different operating conditions.

Specifically, a radial basis function neural network (RBF-NN) has been used to control a doubly fed induction generator (DFIG) WT. This technique is applied to complement a conventional DSC control scheme that calculates the speed reference, considering the electromagnetic torque and aerodynamic parameters, to achieve the MPPT. The objectives of this proposal are to extract the maximum energy despite wind variations and to increase generation efficiency with a rapid response to the fluctuating behavior of the plant. This way, the WT can adapt its operation to the optimal values of the mechanical and electrical variables with greater precision, improving the effectiveness of the MPPT procedure.

The learning algorithm online updates the NN weights to reduce the speed error as the wind speed varies and thus, so does the turbine dynamics. In this way, the controller learns the control that better regulates the torque reference to minimize the speed error. The DSC is used to generate the instantaneous generator speed reference and to obtain the error signals that will feed the NN inputs. The NN then reacts to these random non-linear speed changes and calculates the appropriate electromagnetic torque to stabilize the system. The performance of this hybrid control scheme is compared with the reference OpenFAST controller for a National Renewable Energy Laboratory (NREL) 1.5 MW turbine, giving around 7.87% more power. In addition, the influence of the parameters of the NN and the learning algorithm has been analyzed in detail to explore the effect they have on the control response.

The rest of the paper is structured as follows. Some related works are commented in Section 2. The mathematical model of the WT and the MPPT control approach are described in Section 3. The proposed hybrid neuro-DSC control is explained in Section 4. Section 5 discusses the results of the simulation experiments and analyzes the effects of some parameters on the response. The paper ends with the conclusions and future works.

2. Related Works

In the literature, WT MPPT control is mainly addressed with conventional control methods. Nevertheless, these classical controllers may present a poor response, with some limitations due to the intrinsic non-linear dynamic of the WT. The limitations of these control solutions are shown especially when wind speed experiences variations, according to its random nature. Moreover, the laborious tuning of the parameters and the slow response of some of these control methods are the major drawbacks of their application (Kumar *et al.*, 2019). Some of the traditional techniques apply indirect speed control (ISC). For instance, Pozo *et al.* (2021) use ISC to control a 1.5 MW WT and compare its performance with the controller embedded in FAST. Dbaghi *et al.* (2021) also exploit ISC but in this case they combine it with the backstepping technique. This approach is tested in simulation with a 7.5 kW WT. PID controller is also frequently applied, such as in Camblong *et al.* (2006), where MPPT based on PI DSC is studied and compared with ISC.

Other works that use PID controllers for MPPT propose different techniques to tune the gains. In Azzouz *et al.* (2019) authors use genetic algorithms (GAs) to adjust the gains of a PID to track the maximum power point of a 3.6 MW WT generator. GAs are also used in Belgaid *et al.* (2020) to tune a PI for MPPT, in this case for a smaller WT of 7.5 kW. Particle swarm optimization is used in Bekakra and Attous (2014) to find the optimum parameters of a PID for MPPT. Another optimization technique used is ant-colony algorithm, such as in Mokhtari and Rekioua (2018), where it has been applied to tune the gains of a PID DSC MPPT controller; this approach was later tested in a WT benchmark of 15 kW. Perturb and observe approach has also been proposed for MPPT, some examples of these algorithms can be found in Nurzaman *et al.* (2017), Hossam *et al.* (2019), and Mousa *et al.* (2021).

On the other hand, artificial intelligence techniques are being applied to improve MPPT control. Moreover, they are efficient solutions to solve some limitations of the conventional methods, improving performance, velocity of the response, and capability to manage the complex and non-linear behaviors of the system in this operation region. Fuzzy logic controllers (FLCs) have been designed for optimal WT power production on different types of electrical machines (Naik *et al.*, 2020). To mention some examples, in Yaakoubi *et al.* (2016), authors estimate the reference velocity that ensures the MPPT based on the power and generator speed references for a squirrel cage induction machine. Permanent magnet synchronous generator (PMSG) is widely used in WT, such as in Malobe *et al.* (2020), where the FLC is applied for increasing the robustness of a sliding mode control which faces wind speed variations. In Liu *et al.* (2015), a Takagi-Sugeno FLC is designed for maximum power transfer. In Heshmatian *et al.* (2017), an FLC is proposed which modifies the conventional hill climbing search (HCS) control and provides the appropriate rotational reference speed for MPPT. Using a DFIG WT, in Hou *et al.* (2016) a variable universe FLC is applied considering the active and reactive power in the MPPT problem. In Bhati and Gaur (2020), a supervised fuzzy PID controller is designed to enhance the power extraction of the tip speed ratio (TSR) strategy in a WT with a 2 MW DFIG. In Muñoz *et al.* (2020), DSC is complemented with an FLC for a DFIG WT, regulating the speed with changes in the torque of the machine. The same authors extend this approach considering disturbances in the control signals (Muñoz *et al.*, 2021). In Zouggar *et al.* (2021), ISC is compared with the DSC using both a fuzzy system and a conventional PID that complement the DSC.

Control based on NNs has also shown its good performance and adaptability through various architectures, applied to complex models (Sierra-García & Santos, 2021c). Focusing on the field of WT MPPT, NNs are implemented by using different types of algorithms with a direct or indirect control scheme, being an alternative or complementary solution to conventional techniques for maximum power extraction. To comment some works, in Pathak *et al.* (2016) a backpropagation algorithm is used for indirect current control of the voltage source converter in a wind-diesel generator microgrid. In Sabzevari *et al.* (2017), a NN based on particle swarm optimization is used for wind speed estimation in the control system. This is complemented with an adaptive FLC-PI controller for MPPT operation based on TSR strategy, and it is applied in a small-scale WT. In Rhaili *et al.* (2018), a feedforward backpropagation neural network controller for MPPT is proposed; in contrast to our approach, the controller is trained offline and then online applied to a five-phase PMSG WT, using the nominal power and speed values to extract the MPPT reference. In Davoudi and

Downloaded from https://academic.oup.com/jcde/article/10/1/108/6912246 by guest on 07 July 2024

Kasiri Far (2020), a recurrent NN based on an HCS control method with online learning is proposed. An Elman neural network is applied in Reddy and Ramasamy (2019) to a boost-type Vienna rectifier for the MPPT. In Chandrasekaran *et al.* (2020), a cascaded NN is applied to MPPT control of a PMSG wind power conversion system. In Chojaa *et al.* (2021), a NN is designed to control the optimal WT speed for MPPT, working together with an integral sliding mode control of the DFIG powers.

The RBF-NN in particular has also been used for this type of WT control. For example, Hong *et al.* (2013) combine it with a learning algorithm, a torque observer, and an optimal TSR-based reference speed estimation, which is applied as a sensorless control of a PMSG WT. In Atiqur Rahman and Rahim (2020), a combination of RBF and a control strategy based on optimal ratios is studied to track suitable generator conditions and adjust the reference speed. Unlike our approach, the RBF generates the speed reference and then this is tracked by a PI controller.

As shown in the state of the art, NNs allow to model and control complex systems, and previous studies have used them for MPPT WT control. However, most of them train the networks offline, and the works that design a specific learning algorithm to adjust online the neural weights are scarce. These are the main two contributions of this paper. In this line, the proposal here developed follows the maximum energy extraction for a reference speed that is estimated from the direct measurement of aerodynamic variables, within the DSC scheme. To make it possible, a quick response in the torque is generated to regulate the WT movement. This is achieved by using a compact intelligent controller based on NNs with continuous learning that can adapt to the changes in the system conditions.

3. WT Description

The aerodynamic model of a WT can be expressed in terms of the power the machine harvests from the wind. The mechanical power is determined by a set of parameters that define the WT behavior (Equation 1):

$$P_a = \frac{1}{2}\rho C_p(\lambda,\beta)AV_w^3, \tag{1}$$

where ρ (kg/m^3) is the air density, A (m^2) is the area the blades can sweep, V_w (m/s) is the input wind speed, C_p represents the power coefficient, λ is the TSR, and β (rad) is the pitch angle of the blades.

The power coefficient, C_p, that measures the efficiency of power extraction, depends on TSR and β. A large value indicates a good operation of the WT. That is, the machine is rotating at a suitable speed and the blades are set to an optimal orientation angle in order to capture the maximum energy from the wind. The $C_p(\lambda,\beta)$ function normally is obtained empirically, although it can be mathematically approximated by Equations (2 and 3), where c_1, c_2, c_3, c_4, c_5, c_6, c_7, c_8, and c_9 are a set of constant values that describe the WT, and are usually obtained by identification techniques. This expression illustrates the non-linear dynamics of the turbine. It is influenced by the technical characteristics of the wind device, represented with the parameters c_1–c_9 that define a specific type of WT. This equation is commonly used to obtain a set of curves representing the turbine behavior under different wind conditions. Each curve is obtained with a different pitch angle. In addition, it can be also used to approximate the optimal parameters of the WT—$C_{p.opt}$, λ_{opt}, and β_{opt}—that allow the maximum power extraction:

$$C_p(\lambda,\beta) = c_1\left(\frac{c_2}{\lambda_i} - c_3\beta - c_4\beta^{c_5} - c_6\right)e^{-\frac{c_7}{\lambda_i}} \tag{2}$$

Table 1: Wind turbine parameters.

Parameter	Value
WT capacity	1.5 MW
Number of blades	3
Electrical machine	DFIG
$C_{p.opt}$	0.48
λ_{opt}	7.1
β_{opt}	2°
R	42.75 m
N	72
Rated rotor speed	16.66 rpm
Nominal wind speed	11.5 m/s

$$\lambda_i = \left[\left(\frac{1}{\lambda + c_8\beta}\right) - \left(\frac{c_9}{\beta^3+1}\right)\right]^{-1}. \tag{3}$$

Regarding the TSR, it is calculated using Equation (4), where the blades' length is R (m), ω_r (rad/s) is the rotational speed, and V_w (m/s) the wind speed:

$$\lambda = \frac{\omega_r \cdot R}{V_w}. \tag{4}$$

In this paper, the NREL 1.5 MW onshore WT model is used, for which the maximum operational parameters are specified in Table 1. These values are obtained through aerodynamic simulations with software OpenFAST (by NREL).

3.1. Generator mathematical model

The electrical representation of the DFIG generator type here considered can be described by the Park transform. This representation analyzes the system into a d–q frame, where the electrical variables of voltages and fluxes are decomposed in each of these dimensions. Voltages (V) are modeled with Equation (5) and fluxes (φ) with Equation (6). The subscripts (r) and (s) denote rotor and stator, respectively. The subscripts (d) and (q) denote the component of the d–q frame.

$$\begin{aligned}
V_{ds} &= R_s\, i_{ds} + \frac{d_{\varphi ds}}{dt} - \omega_e\varphi_{qs}\\
V_{qs} &= R_s\, i_{qs} + \frac{d_{\varphi qs}}{dt} + \omega_e\varphi_{ds}\\
V_{dr} &= R_r\, i_{dr} + \frac{d_{\varphi dr}}{dt} - \omega_{slp}\varphi_{qr}\\
V_{qr} &= R_r\, i_{qr} + \frac{d_{\varphi qr}}{dt} + \omega_{slp}\varphi_{dr}
\end{aligned} \tag{5}$$

$$\begin{aligned}
\varphi_{ds} &= L_s\, i_{ds} + M\cdot i_{dr}\\
\varphi_{qs} &= L_s\, i_{qs} + M\cdot i_{qr}\\
\varphi_{dr} &= L_r\, i_{dr} + M\cdot i_{ds}\\
\varphi_{qr} &= L_r\, i_{qr} + M\cdot i_{qs},
\end{aligned} \tag{6}$$

where R (Ω) is the resistance, i (A) is the current, ω_e (rad/s) is the angular speed, ω_{slp} (rad/s) is the slip angular speed, L (H) is the inductance, and M (H) is the mutual inductance.

In the same way, the electromagnetic torque, T_{em}, can be represented in terms of the d–q components, according to Equation (7). Currents and fluxes are the more influential factors regarding the generator torque, and all these elements contribute to the device operation:

$$T_{em} = \frac{3}{2}\,p\frac{M}{L_s}\left(\varphi_{qs}i_{dr} - \varphi_{ds}i_{qr}\right), \tag{7}$$

where p is the pair of poles.

Downloaded from https://academic.oup.com/jcde/article/10/1/108/6912246 by guest on 07 July 2024

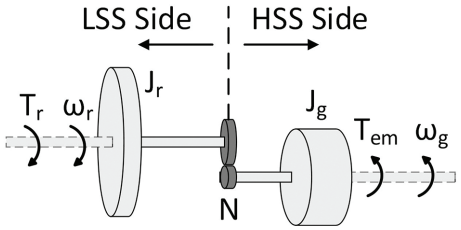

Figure 1: Two-mass powertrain model.

3.2. Mechanical powertrain model

The mechanical system is represented by using a powertrain approximation with a two-mass model (Semrau *et al.*, 2015), as can be seen in Fig. 1.

The low-speed shaft (LSS) at the turbine side and the high-speed shaft (HSS) at the generator side constitute the main elements of the powertrain. The gearbox ratio N (Equation 8) makes it possible to join these two parts, allowing the transmission of movement between the LSS and HSS through a proportional relationship among variables:

$$N = \frac{w_g}{w_r} = \frac{\dot{w}_g}{\dot{w}_r} = \frac{T_r}{T_{em}}. \quad (8)$$

The components of the HSS and LSS sides such as angular accelerations, torques, and inertias, are representative elements of the mechanical model definition (Equation 9):

$$J_r + N^2 J_g = \frac{T_r - NT_{em}}{\dot{\omega}_r}. \quad (9)$$

In these expressions, w_r (rad/s) is the rotor angular velocity and w_g (rad/s) is the generator angular velocity; $\dot{\omega}_r$ (rad/s^2) is the rotor angular acceleration that can be expressed regarding the generator side as $\dot{\omega}_r = \frac{\dot{\omega}_g}{N}$ by using the gearbox ratio, with $\dot{\omega}_g$ as the generator acceleration; T_r (Nm) is the rotor torque and T_{em} (Nm) is the electromagnetic torque; and J_r (Kg · m^2) is the rotor inertia and J_g (Kg · m^2) is the generator inertia. This expression, Equation (9), can be used to estimate the rotor torque from the electromagnetic torque and the rotor angular acceleration.

4. NNs Based MPPT Control Strategy

4.1. Conventional DSC

The conventional DSC control diagram is shown in Fig. 2a. As it is possible to observe, with the DSC strategy, a generator speed reference is continuously calculated in order to track the maximum point of the power curve, MPPT. This generator speed reference is then used as control reference for a WT speed controller. The DSC calculates this speed reference by Equation (10) (Abad *et al.*,

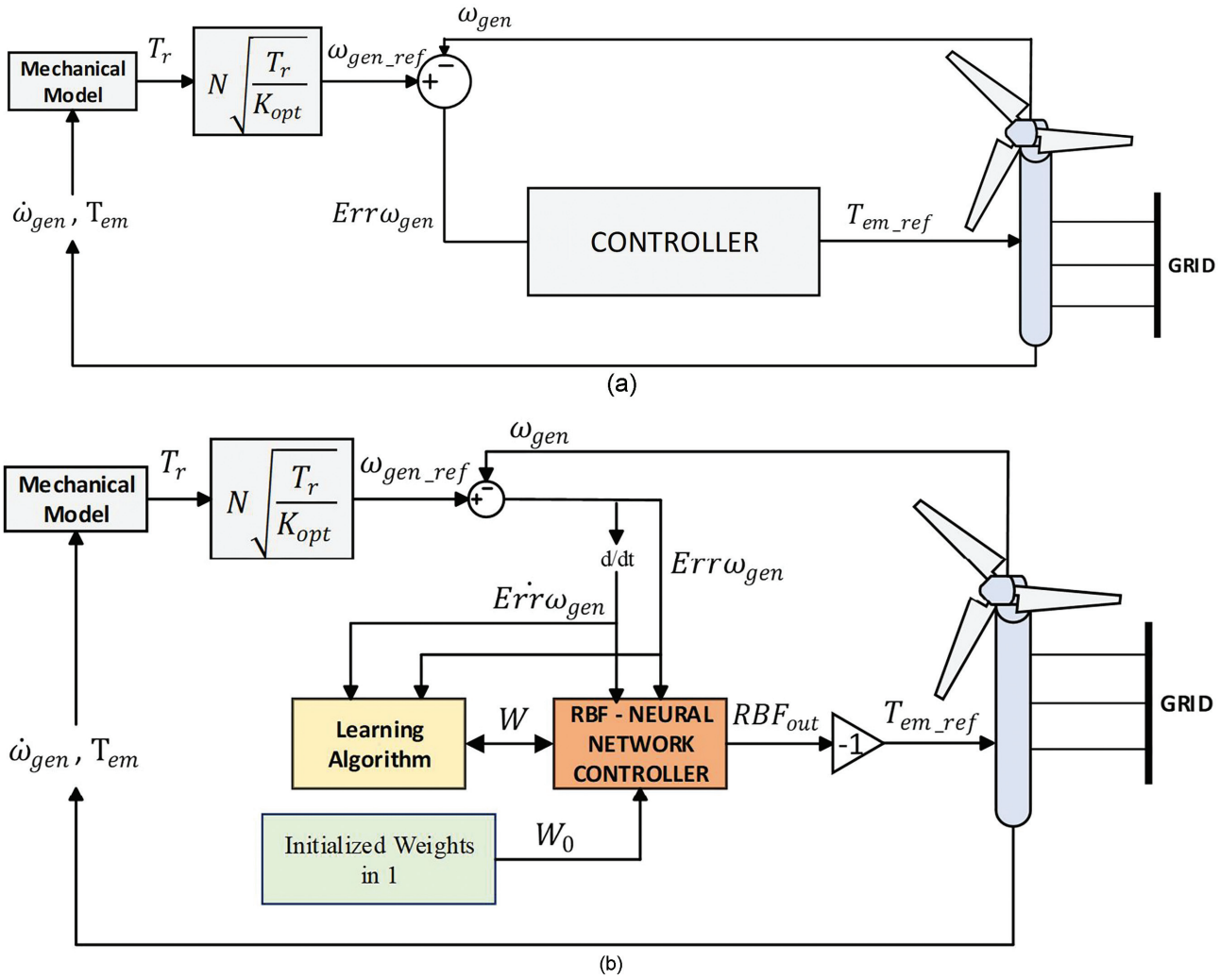

Figure 2: (a) Conventional DSC. (b) DSC improved by NN (DSC-NN).

Downloaded from https://academic.oup.com/jcde/article/10/1/108/6912246 by guest on 07 July 2024

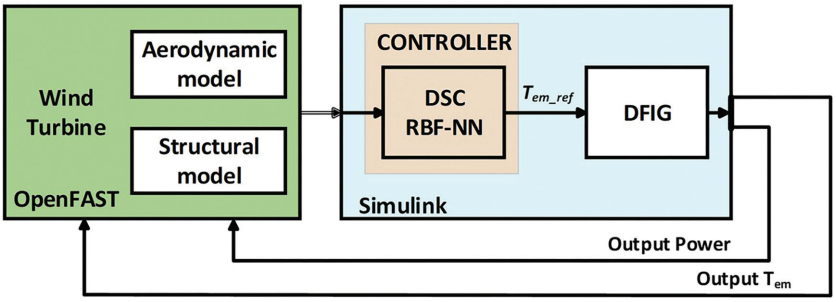

Figure 3: Global simulation scheme.

Table 2: Specifications of the electrical machine.

Parameter	Value
DFIG power	1.5 MW
Rated speed	1200 rpm
Pair of poles, p	3
Frequency	60 Hz
Rotor resistance, $\mathbf{R_r}$	0.99 mΩ
Stator resistance, $\mathbf{R_s}$	1.4 mΩ
Rotor inductance, $\mathbf{L_r}$	0.082 mH
Stator inductance, $\mathbf{L_s}$	0.09 mH

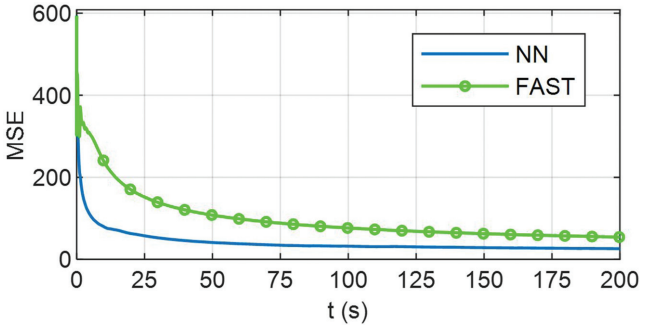

Figure 4: MSE for the best RBF-NN configuration.

2011; Camblong *et al.*, 2006). Once the desired generated speed is obtained, the speed error is calculated and the speed controller is in charge of obtaining the electromagnetic torque reference to follow the speed reference without error. This speed controller is normally implemented by a PID regulator, although other approaches can be used.

The DSC uses the rotor torque T_r and the optimal constant K_{opt} to obtain the generator speed reference, ω_{gen_ref} (Equation 10). With this aim the rotor torque is usually indirectly estimated from the generator torque and the rotor acceleration, using Equation (9). On the other hand, the optimal constant K_{opt} (Equation 11) is defined from the optimum TSR, i.e., λ_{opt}, and the optimum C_p, $C_{p.opt}$; the blades length is R and the air density is ρ:

$$\omega_{gen\_ref} = N\sqrt{\frac{T_r}{K_{opt}}} \tag{10}$$

$$K_{opt} = \frac{1}{2}\,\pi\rho C_{p.opt}\frac{R^5}{\lambda_{opt}^3}. \tag{11}$$

4.2. DSC improved by NNs

In order to generate the reference of the electromagnetic torque for the MPPT strategy, an RBF-NN whose weights are dynamically updated by a ULA is designed. This improved DSC control architecture is shown in Fig. 2b. In short, the speed controller in Fig. 2a is replaced by an RBF-NN.

In this DSC-NN control scheme, the speed error, $Err\omega_{gen}$, and its derivative, $Err\dot{\omega}_{gen}$, are the inputs of the RBF-NN. The $Err\omega_{gen}$ is the difference between the reference speed ω_{gen_ref} (Equation 10), and the actual generator speed, ω_{gen}. The output of the neuro controller is the reference of the electromagnetic torque, T_{em_ref}, that allows the WT to reach the maximum power point. A reference power, P_{ref}, can be obtained with Equation (12). This control is executed at each control period, T_c:

$$P_{ref} = T_{em\_ref} * \omega_{gen}. \tag{12}$$

The implementation of this control strategy involves three main components. The RBF-NN controller that represents the mapping function between the speed error and the torque reference, which implements the control law to follow the desired speed; the learning algorithm i.e., a function that updates the neural weights during the WT system operation, so the NN online learns this control law; and finally, the weights initialization block that introduces a uniform value for all weight of the neurons, initially set to 1 at the beginning of the control loop, but which are continuously updated by the learning procedure.

In order to apply the RBF network, the input variables are discretized in a bi-dimensional space, limited by the maximum and minimum speed error and by a defined range of the derivative speed error. In the simulations, these ranges are set to [−1200, 1200] rad/s and [−400, 400] rad/s^2, respectively. Within the range of these inputs, an equally distributed grid is created to locate the centers of the RBF neurons. Hence, the distance between cells changes accordingly to the number of neurons. The generation of this grid has been inspired and adapted from the pitch control presented in Sierra-García and Matilde (2020). Once the grid is generated, the centers of the neurons are located at the intersection of the grid division lines. The total number of neurons is given by Equation (13):

$$N_T = (N_x + 1)\cdot(N_y + 1), \tag{13}$$

where N_x and N_y are the number of grid cells of error speed and its derivative, respectively. The center of the i-neuron is denoted with the pair (c_{ix}, c_{iy}).

The output of the RBF can be approximated by Equation (14), as a sum of exponential functions multiplied by an adjustment factor W_i, which represents the i-neuron weight:

$$RBF_{out} = \sum_{i=1}^{N_T} W_i \cdot e^{-\left(\frac{normDist\left(c_{ix},\, c_{iy}, Err\omega_{gen},\, Err\dot{\omega}_{gen}\right)}{\delta}\right)}, \tag{14}$$

Downloaded from https://academic.oup.com/jcde/article/10/1/108/6912246 by guest on 07 July 2024

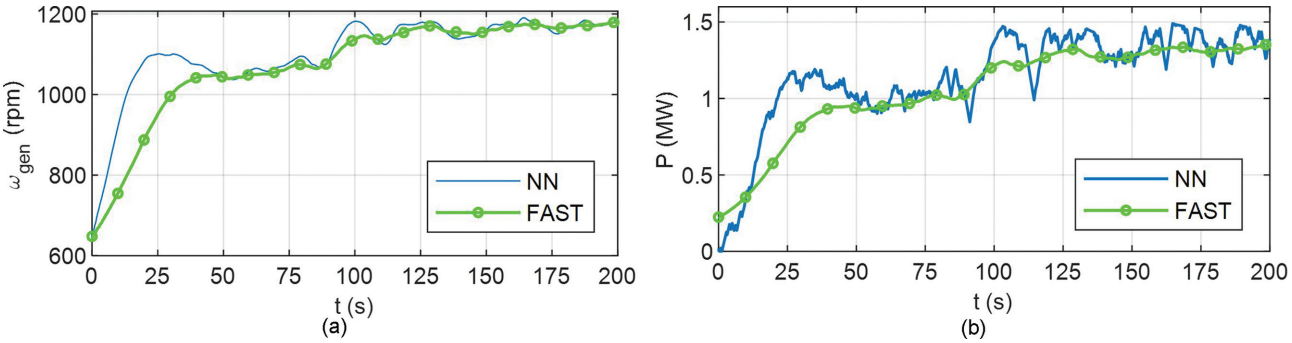

Figure 5: RBF-NN control response. (a) Generator speed. (b) Output power.

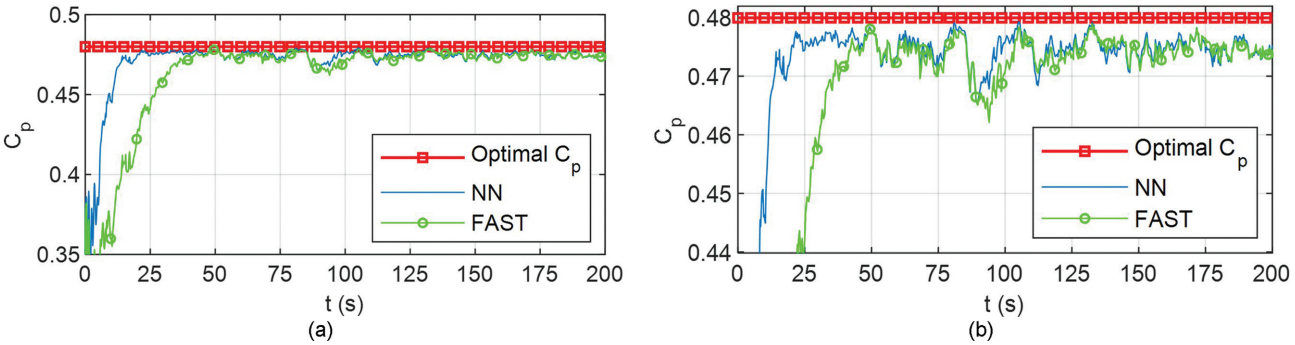

Figure 6: Power coefficient with the best RBF-NN configuration. (a) Original response. (b) Zoomed response.

Table 3: Sampled simulation results.

Time (s)	DSC-NN				OpenFAST			
	MSE	ω_{gen} [rad/s]	P [MW]	C_p	MSE	ω_{gen} (rad/s)	P (MW)	C_p
25	57.372	1100.8	1.1303	0.4745	151.810	950.8	0.7087	0.4423
50	41.174	1044.4	1.0232	0.4778	107.840	1042.7	0.9349	0.4777
75	34.450	1079.1	1.0319	0.4724	88.236	1067.2	1.0023	0.4707
100	32.110	1181.7	1.3747	0.4759	76.480	1137.9	1.2150	0.4709
125	30.414	1178.6	1.3737	0.4748	68.447	1166.9	1.3104	0.4735
150	28.516	1160.0	1.2955	0.4731	62.557	1156.5	1.2755	0.4726
175	27.139	1155.6	1.4335	0.4740	58.002	1165.5	1.3056	0.4751
200	26.034	1188.0	1.3882	0.4753	54.313	1181.0	1.3582	0.4746

Table 4: Efficiency indicators

	eff_{C_p}	eff_P	P_{avg} (MW)
DSC-NN	98.06%	76.38%	1.1463
OpenFAST	96.24%	70.77%	1.0627

where δ is the width of the RBF neuron and *normDist* is the normalized distance between the center of a neuron (c_{ix}, c_{iy}) and the point defined by the error pair ($Err\omega_{gen}$, $Err\dot{\omega}_{gen}$), i.e., Equation (15):

$$normDist = \sqrt{\frac{(c_{ix} - Err\omega_{gen})^2}{Err\omega^2_{gen\_max}} + \frac{(c_{iy} - Err\dot{\omega}_{gen})^2}{Err\dot{\omega}^2_{gen\_mac}}}. \quad (15)$$

As it is possible to realize, the distance of the pair ($Err\omega_{gen}$, $Err\dot{\omega}_{gen}$) to a specific neuron is related to the effect that the neuron has on the network output. The smaller the distance, the closer to 1 the neural output is, following a negative exponential function curve. The final RBF output is obtained by the addition of the output of all neurons weighted by their corresponding coefficients W_i.

Because of the inverse relationship between the generator speed and the electromagnetic torque (Equations 9 and 12), the RBF output must be inverted. Therefore, RBF_{out} is multiplied by −1 and the resultant reference electromagnetic torque is obtained.

4.3. Unsupervised learning algorithm

To ensure the NN executes the proper control law, a learning process that adjusts the neuron weights in order to reduce the speed error while the system is working has been implemented. The ULA updates the weights taking into account the speed error. If this error grows, the weights of the network are increased; this increases the output of the NN, which reduces the electromagnetic torque and raises the generator speed. This way the speed error is reduced, and the control loop is established. The expression that summarizes this NN learning process in the time domain t is given

Downloaded from https://academic.oup.com/jcde/article/10/1/108/6912246 by guest on 07 July 2024

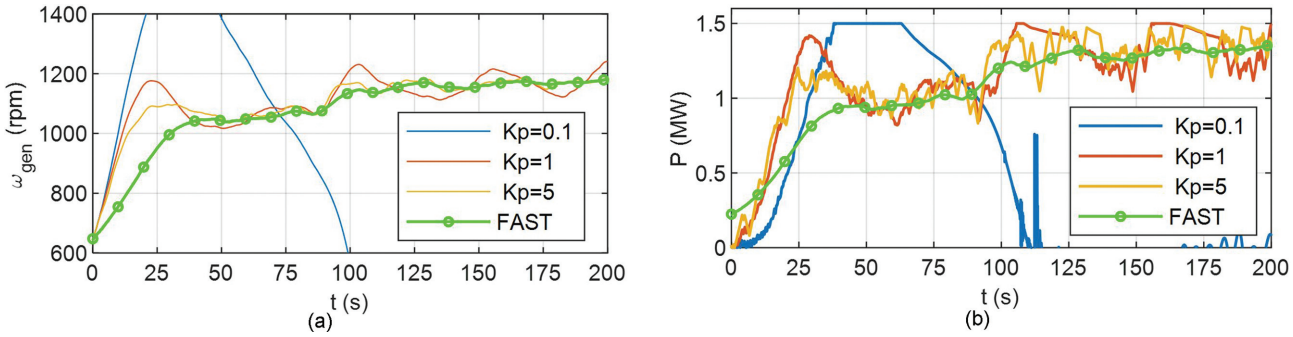

Figure 7: System response with K_p variations. (a) Generator speed. (b) Output power.

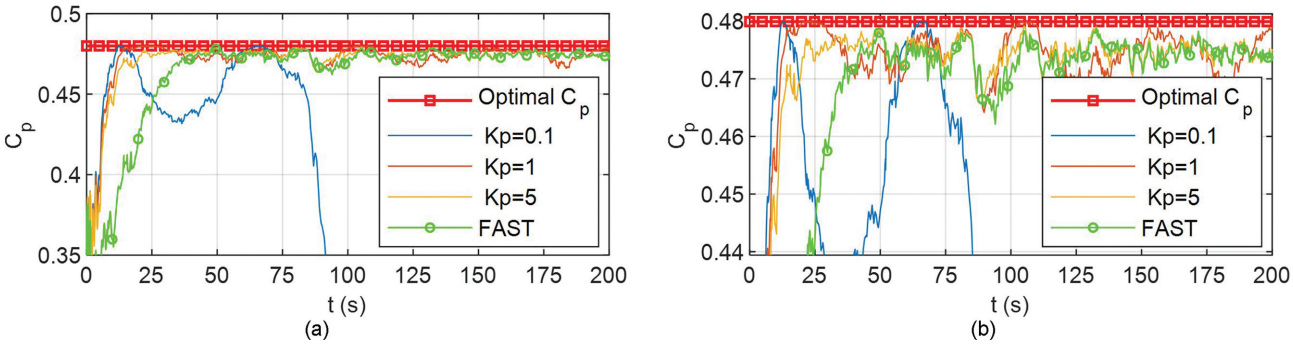

Figure 8: Power coefficient with K_p variations. (a) Original response. (b) Zoomed response.

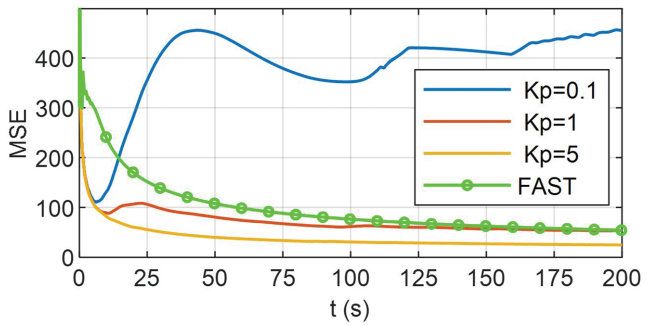

Figure 9: MSE with K_p variations.

by Equation (16):

$$W_j\ (t_i) = W_j\ (t_{i-1}) + \mu \cdot \left(K_p Err\omega_{gen}\ (t_i) + K_d Err\dot{\omega}_{gen}\ (t_i)\right) \cdot e^{-\left(\frac{normDist}{\delta}\right)}, \tag{16}$$

where K_p and K_d are constants that modulate the contribution of the speed error and its derivative in the learning, and μ is the learning rate.

As each neuron has a different contribution to the network output depending on the distance (Equations 14 and 15), the ULA also considers the distance of each neuron to regulate the increment of each weight.

As said before, the variation of the weights is related to the error of the generator speed. Large errors indicate that the output of the NN is far from the optimum value, so the increments should be large. On the contrary, when the error is zero it means that the RBF output is correct and therefore, the weights must be kept.

In supervised learning algorithms such as gradient descent backpropagation, the expected output of the network is known *a priori*. This way, the algorithm calculates the weights to minimize the error between the expected output (target) and the real output of the network. However, in our case, we do not know the expected output of the network, as we do not know *a priori* the mapping function between the speed error and the generator torque reference. This relationship is the control law, and is learnt online while the system is working. For this reason, this learning algorithm is unsupervised.

In summary, the learning is shown in the adaptation of the neural weights that is done considering the input speed errors, resulting in the minimization of the generator speed error by the output variable of the neuro-controller.

5. Discussion of the Results

Several simulations of the proposed DSC-NN control algorithm were run. Results are compared with the embedded OpenFAST MPPT control torque. The simulations last 200 s. The simulation step specified in OpenFAST and Simulink is constant and is set to 5 ms. The wind speed follows a random profile between 9 and 11.5 m/s, as the specific WT used operates in the MPPT region for this wind speed range. The results have been obtained using Matlab/Simulink software for the control algorithm and OpenFAST for the realistic NREL 1.5 MW WT simulation. The global simulation scheme used is shown in Fig. 3.

As it is possible to see in this Fig. 3, the controller and the DFIG generator models are simulated in Simulink. On the other hand, the aerodynamics and the structural model of the WT are simulated in OpenFAST.

The representative parameters of the generator used in this work are listed in Table 2.

In addition, to evaluate the influence of the parameters of the controller and the learning algorithm on the WT response,

Downloaded from https://academic.oup.com/jcde/article/10/1/108/6912246 by guest on 07 July 2024

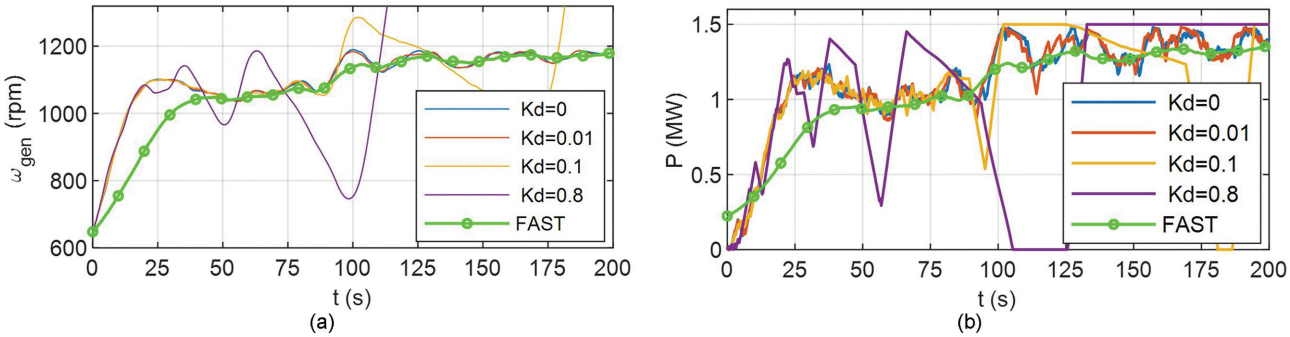

Figure 10: System response with K_d variations. (a) Generator speed. (b) Output power.

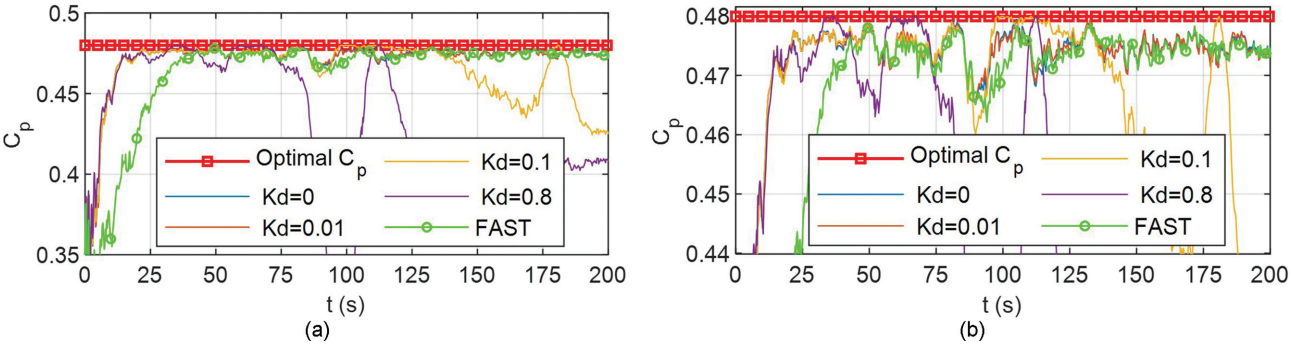

Figure 11: Power coefficient with K_d variations. (a) Original response. (b) Zoomed response.

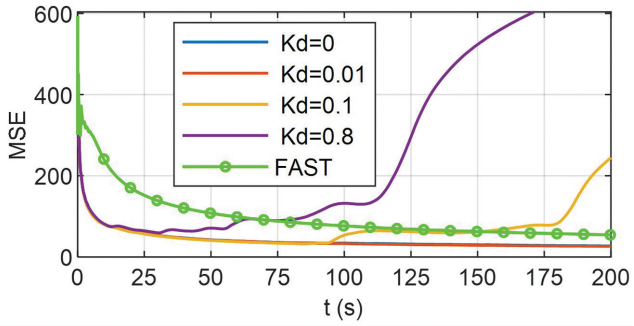

Figure 12: MSE with K_d variations.

different simulations have been carried out varying the configuration parameters. In Section 5.1, the results of the best configuration found are discussed. From Section 5.2 on, an analysis of the influence of these parameters is presented.

5.1. Evaluation of the control performance

The best configuration found in terms of minimum mean squared of the speed generator error (MSE) and maximum generated power is described below. The RBF-NN has 121 neurons and width $\delta = 0.1$; the learning rate μ is set to 0.2; the control period T_c is 20 ms. The proportional and derivative gains of the implemented PD controller (K_p, K_d) are (3, 0.05).

We used iterative simulations, changing the value of these parameters and measuring the mean square error (MSE). According to this metric, the gains were updated, increasing or decreasing their values to decrement the error response. Finally, the configuration (K_p, K_d) with smallest MSE was selected. These controller gains give a response that meets the MPPT control requirements and maintains the WT variables within the optimal operating ranges.

Figure 4 compares the MSE curve obtained with DSC-NN (blue line), and with OpenFAST (green line). It is possible to see how with the DSC-NN the error decreases very quickly, mainly the first 25 s, reaching a smaller value than with the OpenFAST MPPT. Thus, the DSC-NN can be considered better regarding the system dynamics, with a more accurate and quicker response. This means that the NN control algorithm can provide a suitable electromagnetic signal to regulate the generator, and thus the turbine speed is rightly adjusted. The system performance is then adjusted to the dynamic changes of the device and the input wind speed.

As a result of the MSE decrease, the evolutions of the generator speed, Fig. 5a, and output power, Fig. 5b, also show that the proposed DSC-NN control approach works well. Indeed, the neuro-control strategy achieves the rated values, and in terms of output power, although the response is a bit more oscillatory and with noise, the amount of power captured and generated using this controller is bigger. The control and learning actions allow fast reaction of the system in order to regulate the speed and maintain the optimum TSR. Thus, the relationship between turbine rotor speed and wind speed remains balanced. In this process, those changes produce continuous variations in the power which justify its behavior. Finally, this adaptation to the system dynamics means a higher level of power production.

In the same way, regarding the C_p curve (Fig. 6), the DSC-NN control reaches the optimal C_p reference in around 10 s, and then it keeps that value along the simulation, making it possible to generate more power than with the OpenFAST control, that requires around 40 s to get the reference; i.e., the neuro-control is 75% faster. Thus, the DSC-NN control allows tracking the maximum power point with greater precision and speed. This proves its efficiency in the operating region of the MPPT, where the interaction

Downloaded from https://academic.oup.com/jcde/article/10/1/108/6912246 by guest on 07 July 2024

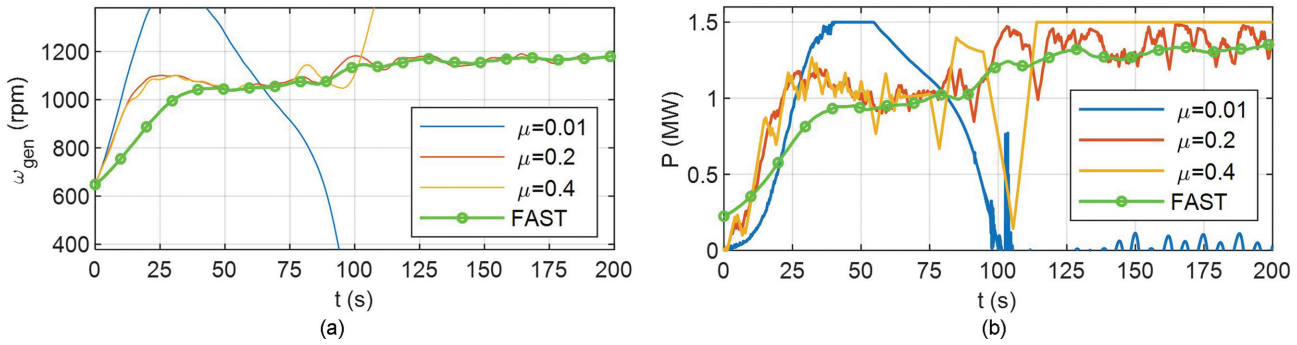

Figure 13: System response with learning rate variations. (a) Generator speed. (b) Output power.

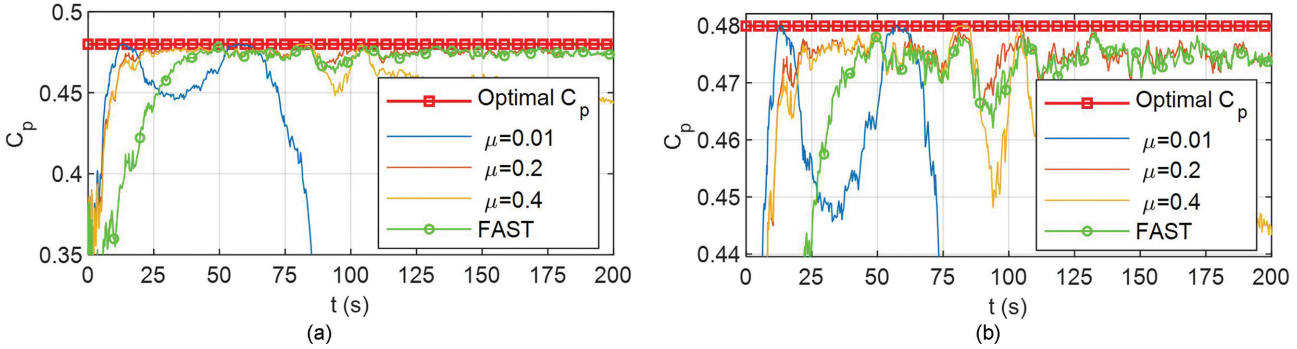

Figure 14: Power coefficient with learning rate variations. (a) Original response. (b) Zoomed response.

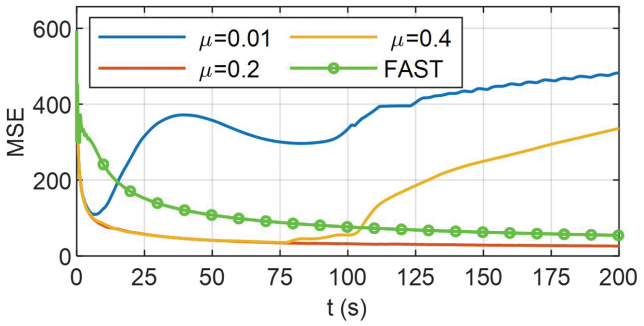

Figure 15: MSE with learning rate variations.

between the variables of the WT is controlled more effectively. Fig. 6b shows a zoom of the C_p curve in order to observe the differences between both responses.

Table 3 summarizes the obtained results. The values of the variables are acquired every 25 s to make easier observe the numerical differences between the DSC-NN control and the OpenFAST controller. The results show that the implementation of the DSC-NN control presents some advantages, as it extracts more power over time, showing a higher efficiency according to the higher values of the power coefficient kept along the simulation. The MSE response also proves that the proposed controller is more accurate; indeed, the MSE is approximately half of the error given by the OpenFAST controller.

As another indicator of efficiency, the closeness to the nominal C_p and rated WT power are calculated using Equation (17):

$$eff_A = \frac{\sum_{i=1}^{n} \frac{A_i}{A_{max}}}{n} \cdot 100\%, \tag{17}$$

where A denotes the variable to be analyzed, C_p or power (P). The number of elements is n, and max indicates the optimal or nominal value of the variable.

Additionally, the generated average power P_{avg} is obtained for the simulation time T_{sim} of the experiments, using Equation (18):

$$P_{avg} = \frac{1}{T_{sim}} \int P_{out}(t) \cdot dt. \tag{18}$$

Table 4 shows the metrics defined by Equations (17 and 18) that measure the efficiency of the MPPT controllers.

These indicators reflect that proposed neuro-controller gives more energy, specifically, 7.87% more than the OpenFAST MPPT control.

In short, the neural control system is more effective, following the reference with smaller error. The learning algorithm allows the controller to quickly adapt to the plant and operate with good results in the MPPT region.

5.2. Influence of the parameters of the learning algorithm

To select the best NN configuration, the influence of the learning algorithm parameters has been analyzed. In addition, some knowledge can be obtained regarding the tuning of the controller when some values of the WT dynamics change.

5.2.1. K_p and K_d variation

To establish the variation range of the tuning parameters of the PD controller, the influence of the proportional gain K_p is evaluated varying it between 0.1 and 5. For these values of K_p, Fig. 7a shows the generator speed and Fig. 7b the output power. The power coefficient is represented in Fig. 8, and the MSE in Fig. 9. According to these graphics, when the proportional gain increases the system response improves, i.e., the error is reduced and the speed

Downloaded from https://academic.oup.com/jcde/article/10/1/108/6912246 by guest on 07 July 2024

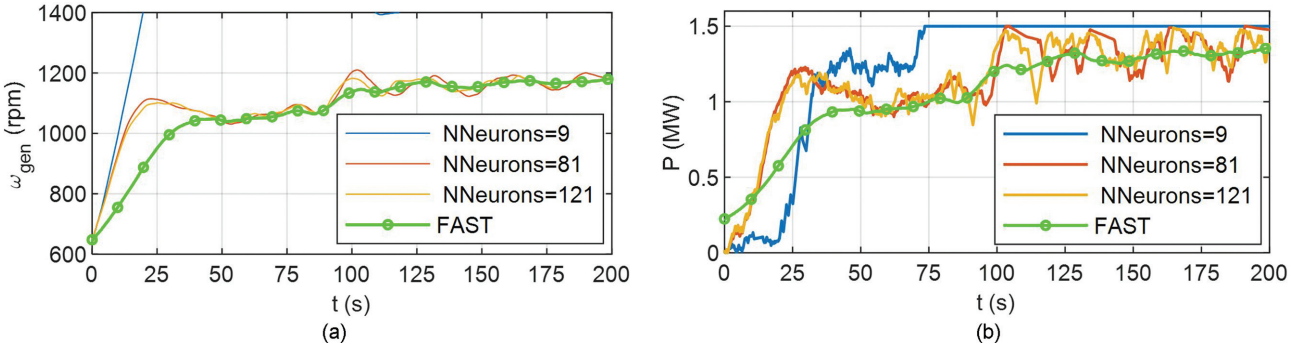

Figure 16: System response with variations of the number of neurons. (a) Generator speed. (b) Output power.

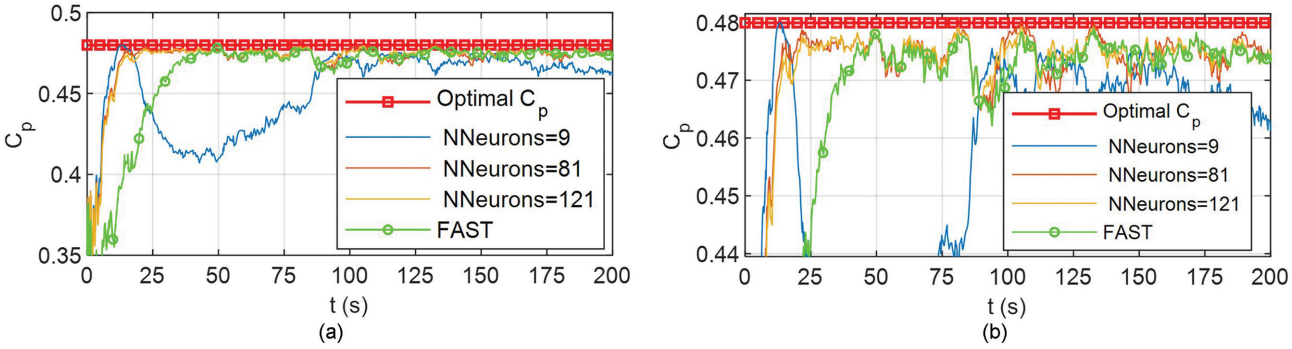

Figure 17: Power coefficient with variations of the number of neurons. (a) Original response. (b) Zoomed response.

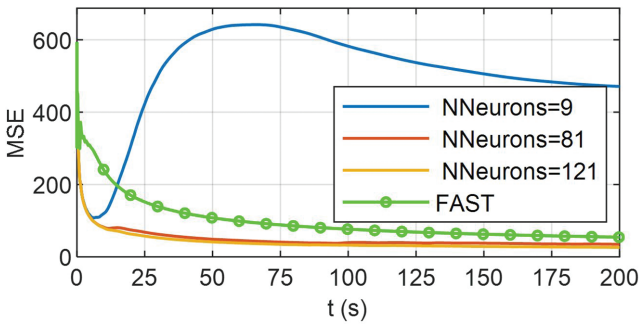

Figure 18: MSE with variations of the number of neurons.

and C_p values are closer to their optimal values, so the generated power reaches higher values. With small values of K_p, the system cannot be controlled (Fig. 9). If the value is well selected, the controller improves the system response and acquires more stability and better performance.

Except for very small values of K_p, the MSE error with the NN algorithm is much smaller than with the OpenFAST control.

Increasing slightly the value of the K_d tuning parameter, the system response is smoother and more stable, and the error is reduced. However, high values of this parameter increase the oscillations of the generator speed (Fig. 10a) and thus, the other variables.

Figure 10b shows the necessity of adjusting the derivative gain to small values so not to make the output power too oscillatory. The same happens with the power coefficient (Fig. 11a and b). Furthermore, aiming to reduce control effort and computational complexity, this gain can be even set to 0. Its influence on the final results is negligible.

The MSE (Fig. 12) is still very low for small values of this parameter but along the simulation it gets worse for higher values.

5.2.2. *Learning rate variation*

The learning rate directly influences the control quality. Very small or very large values may cause erroneous results while a value around 0.2–0.4 makes the control effective. This may be explained as this parameter multiplies the proportional and the derivative PD gains, and it has been shown that small K_p values or large K_d values increase the oscillation of the response. Figures 13–15 are clear evidence of this. As it can be seen, $\mu = 0.2$ is the best value found with the simulations. In addition, the DSC-NN controller gives better response than the OpenFAST torque control with this learning rate.

5.3. Influence of the RBF-NN configuration

5.3.1. *Number of neurons*

The number of neurons of the RBF-NN is also a factor to be taken into account as it also has some effects on the system response. The generator speed, output power, C_p and MSE are shown in Figs. 16–18, respectively, when the number of neurons of the RBF-NN varies. In general, more neurons improve the control. In this case, with $11 \times 11 = 121$ neurons, the controller generates an adequate output for each variable involved in the control scheme. On the opposite, with a small number of neurons the controller cannot work efficiently or even the WT cannot be controlled, as in the simulated case with $3 \times 3 = 9$ neurons. In this particular case, the power results are saturated to the rated 1.5 MW for visualization purposes, to see how the variables evolve with these changes. But the fact is that with a specific number of neurons below a threshold, the system variables are out of the appropriate

Downloaded from https://academic.oup.com/jcde/article/10/1/108/6912246 by guest on 07 July 2024

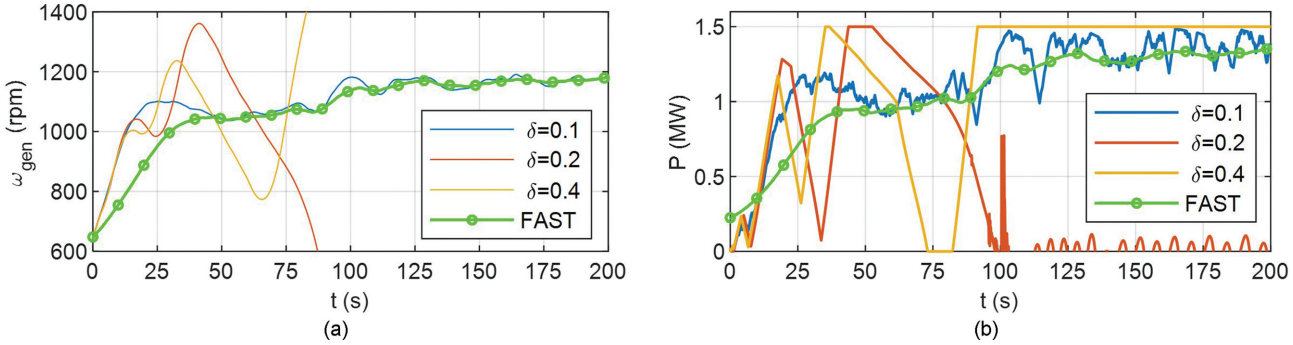

Figure 19: System responses with activation function weight variations. (a) Generator speed. (b) Output power.

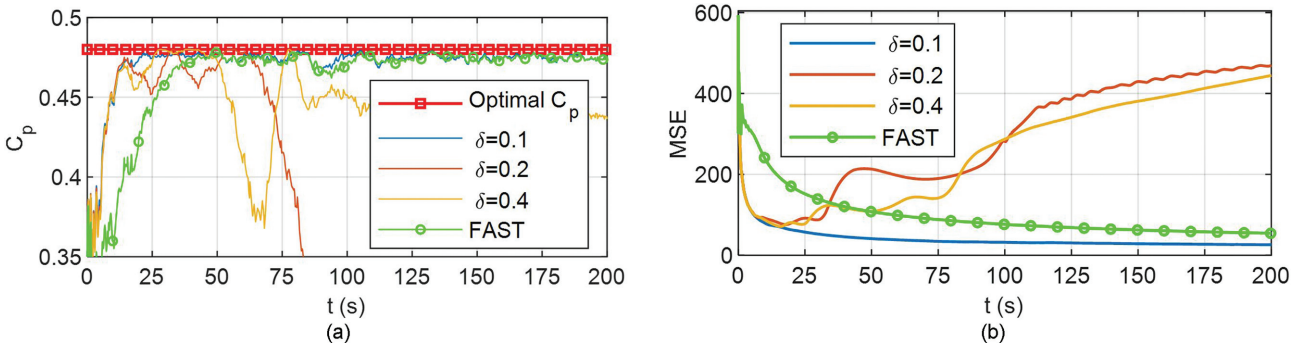

Figure 20: Responses with activation function weight variations. (a) Power coefficient. (b) MSE.

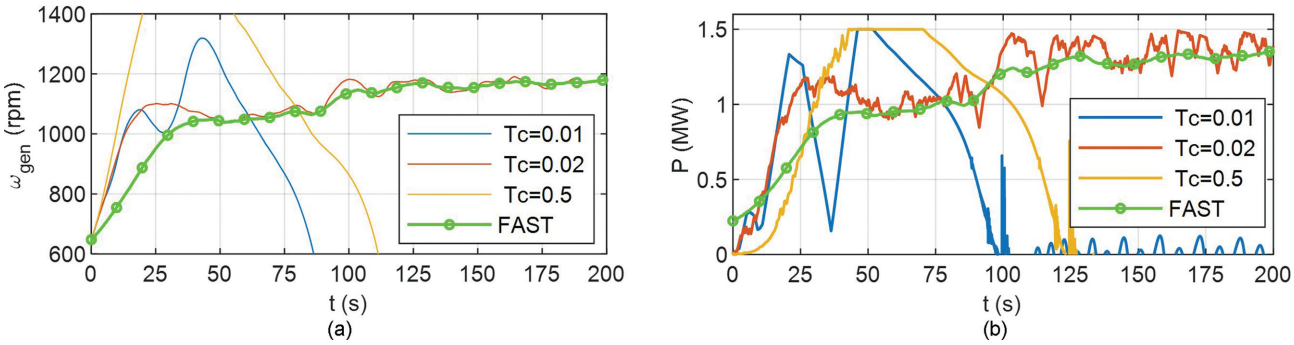

Figure 21: Responses with control period variations. (a) Generator speed. (b) Output power.

ranges, concluding that the control does not work for that small number of neurons.

In terms of comparison with other controllers, results with the NN are more accurate, faster, and with smaller error than with the OpenFAST control when this factor is set to a suitable number. In addition, in order to reduce computational time, the number of neurons was set to $9 \times 9 = 81$ as it is a good choice and the differences with using 121 neurons are almost negligible.

5.3.2. *Activation function weight*

The influence of the activation function weight is clear. As expected, a small value helps the control to work more efficiently, as it improves the accuracy of the mapping function implemented by the NN. On the contrary, large values of this parameter cause neurons whose center is far from the input influence the network output, and thus, distort the results. Indeed, large values produce bigger errors and oscillations. The control variables considered in this analysis are shown in Figs. 19 and 20, when activation function weight changes. The value of 0.1 generates the best system response.

5.4. Influence of the control period

Finally, the influence of the control period is tested and shown in Figs. 21–23. If this parameter grows too much, the control is not able to adapt to the dynamic behavior of the WT with the required speed. This effect negatively influences the results. In the opposite case, when the control period is set to a very small value, the control becomes too oscillating and the effects are similar in terms of losing control. With an appropriate value ($T_c = 0.02$), the controller adapts to the system dynamics and gives good performance.

6. Conclusions and Future Works

In this work, the MPPT control of a WT is addressed with a control architecture that combines conventional DSC with an RBF-NN. A ULA is applied so the controller learns online how to regulate the

Downloaded from https://academic.oup.com/jcde/article/10/1/108/6912246 by guest on 07 July 2024

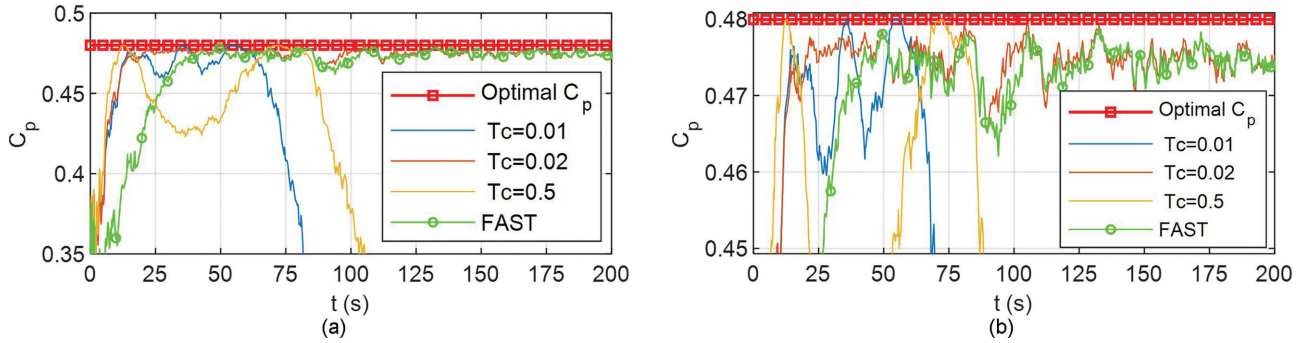

Figure 22: Power coefficient with control period variations. (a) Original response. (b) Zoomed response.

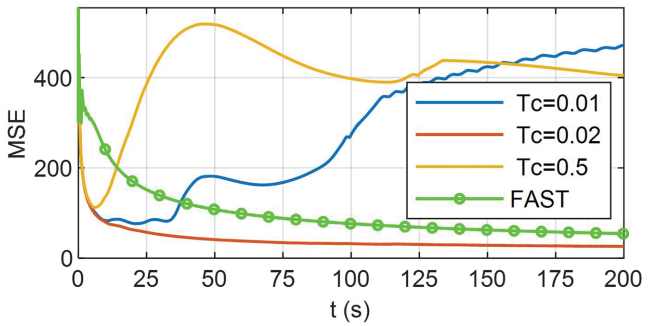

Figure 23: MSE with control period variations.

generator torque reference in order to minimize the speed error. This hybrid intelligent control scheme allows the control to track the required generator rotational speed and thus, to reach the maximum wind energy generation. This way, the controller reacts faster and it better follows the optimal power point so to maximize the energy conversion and to improve the system responses facing wind speed variations. The proposed neural controller has been compared with the torque controller included in OpenFAST, giving better results according to different metrics, which validates the effectiveness of the proposed intelligent approach. Indeed, the neural-based control strategy provides around a 7.87% more power.

In addition, the influence of the control related parameters on the system response has been analyzed. In general, the increment of the PD gains K_p and K_d improves the system response, although they cannot be very high to avoid oscillations. The learning rate has a similar behavior; very small values make the system not learn but very large ones make it more oscillatory.

As future work, we may highlight the evaluation of this approach using recurrent NNs and the implementation and testing of this hybrid control strategy in a small WT prototype.

Acknowledgments

This work has been partially supported by the Spanish Ministry of Science and Innovation under the project MCI/AEI/FEDER number RTI2018-094902-B-C21 and PDI2021-123543OB-C21.

References

Abad, G., Lopez, J., Rodriguez, M., Marroyo, L., & Iwanski, G. (2011). *Doubly fed induction machine: Modeling and control for wind energy generation*. John Wiley & Sons.

Atiqur Rahman, M. M., & Rahim, A. H. M. A. (2020). Design and testing of an MPPT algorithm using an intelligent RBF neural network and optimum relation based strategy. In *Proceedings of the IEEE Region 10 Symposium (TENSYMP)* (pp. 1245–1248). https://doi.org/10.1109/TENSYMP50017.2020.9230807.

Azzouz, S., Messalti, S., & Harrag, A. (2019). Innovative PID-GA MPPT controller for extraction of maximum power from variable wind turbine. *Przegląd Elektrotechniczny*, **95**. https://doi.org/10.15199/48.2019.08.26.

Bekakra, Y., & Attous, D. B. (2014). Optimal tuning of PI controller using PSO optimization for indirect power control for DFIG based wind turbine with MPPT. *International Journal of System Assurance Engineering and Management*, **5**, 219–229. https://doi.org/10.1007/s13198-013-0150-0.

Belgaid, Y., Helaimi, M. H., Taleb, R., & Youcef, M. B. (2020). Optimal tuning of PI controller using genetic algorithm for wind turbine application. *Indonesian Journal of Electrical Engineering and Computer Science*, **18**, 167–178. https://doi.org/10.11591/ijeecs.v18.i1.pp167-178.

Bhati, S., & Gaur, P. (2020). Hybrid fuzzy-PID based MPPT enhancement of grid-Connected DFIG wind energy eystem with TLBO optimization, *International Journal of Engineering Research & Technology (IJERT)*, **9**. https://doi.org/10.17577/IJERTV9IS070213.

Camblong, H., de Alegria, I., Rodriguez, M., & Abad, G. (2006). Experimental evaluation of wind turbines maximum power point tracking controllers. *Energy Conversion and Management*, **47**, 2846–2858. https://doi.org/10.1016/j.enconman.2006.03.033.

Chandrasekaran, K., Mohanty, M., Golla, M., Venkadesan, A., & Simon, S. P. (2020). Dynamic MPPT controller using cascade neural network for a wind power conversion system with energy management. *IETE Journal of Research*, **68**(5), 3316–3330. https://doi.org/10.1080/03772063.2020.1756934.

Chojaa, H., Derouich, A., Chehaidia, S. E., Zamzoum, O., Taoussi, M., & Elouatouat, H. (2021). Integral sliding mode control for DFIG based WECS with MPPT based on artificial neural network under a real wind profile. *Energy Reports*, **7**, 4809–4824. https://doi.org/10.1016/j.egyr.2021.07.066.

Davoudi, M., & Kasiri Far, A. (2020) Recurrent neural network based MPPT control of grid connected DFIG for wind turbine. *Wseas Transactions on Computer Research*, **8**, 1–10. https://doi.org/10.37394/232018.2020.8.1.

Dbaghi, Y., Farhat, S., Mediouni, M., Essakhi, H., & Elmoudden, A. (2021). Indirect power control of DFIG based on wind turbine operating in MPPT using backstepping approach. *International Journal of Electrical and Computer Engineering*, **11**, 1951. https://doi.org/10.11591/ijece.v11i3.pp1951-1961.

Hemanth Kumar, M., Saravanan, B., Sanjeevikumar, P., & Blaabjerg, F. (2018). Review on control techniques and methodologies for

Downloaded from https://academic.oup.com/jcde/article/10/1/108/6912246 by guest on 07 July 2024

maximum power extraction from wind energy systems. *IET Renewable Power Generation*, **12**, 1609–1622. https://doi.org/10.1049/iet-rpg.2018.5206.

Hernández, A. G., & Santos, S. P. (2021). Modelling and experimental validation of aging factors of photovoltaic solar cells. *IEEE Latin America Transactions*, **19**, 1270–1277. https://doi.org/10.1109/TLA.2021.9475857.

Heshmatian, S., Kazemi, A., Khosravi, M., & Khaburi, D. A. (2017). Fuzzy logic based MPPT for a wind energy conversion system using sliding mode control. In *Proceedings of the 2017 8th Power Electronics, Drive Systems & Technologies Conference (PEDSTC)* (pp. 335–340). https://doi.org/10.1109/pedstc.2017.7910348.

Hong, C.-M., Chen, C.-H., & Tu, C.-S. (2013). Maximum power point tracking-based control algorithm for PMSG wind generation system without mechanical sensors. *Energy Conversion and Management*, **69**, 58–67. https://doi.org/10.1016/j.enconman.2012.12.012.

Horno, L. D., Somolinos, J. A., Segura, E., & Morales, R. (2020). A new proposal for the closed-loop orientation control of a windfloat turbine system. *Journal of Marine Science and Engineering*, **9**, 26. https://doi.org/10.3390/jmse9010026.

Hossain, M., & Ali, M. (2022). Future research directions for the wind turbine generator system. *Renewable and Sustainable Energy Reviews*, **49**, 481–489. https://doi.org/10.1016/j.rser.2015.04.126.

Hossam, H. H., Youssef, A.-R., & Essam, E. M. M. (2019). Improved perturb and observe MPPT algorithm of multi-phase PMSG based wind energy conversion system. In *Proceedings of the 2019 21st International Middle East Power Systems Conference (MEPCON)* (pp. 97–102). https://doi.org/10.1109/MEPCON47431.2019.9008004.

Hou, G., Jiang, Z., Yang, Y., & Zhang, J. (2016). Variable universe fuzzy controller used in MPPT based on DFIG wind energy conversion system. In *Proceedings of the 2016 Chinese Control and Decision Conference (CCDC)* (pp. 5871–5875). IEEE. https://doi.org/10.1109/CCDC.2016.7532048.

Kumar, R., Agrawal, H. P., Shah, A., & Bansal, H. O. (2019). Maximum power point tracking in wind energy conversion system using radial basis function based neural network control strategy. *Sustainable Energy Technologies and Assessments*, **36**, 100533. https://doi.org/10.1016/j.seta.2019.100533.

Liu, P., Yang, W. T., Yang, C. E., & Hsu, C. L. (2015). Sensorless wind energy conversion system maximum power point tracking using Takagi-Sugeno fuzzy cerebellar model articulation control. *Applied Soft Computing* **29**, 450–460. https://doi.org/10.1016/j.asoc.2015.01.019.

Lobo, K., & Santos, M. (2019). Modeling and simulation of hydroelectric projects with reservoirs. *IEEE Latin America Transactions*, **17**, 1588–1597. https://doi.org/10.1109/TLA.2019.8986436.

Malobe, P., Djondine, P., Eloundou, P., & Ndongo, H. (2020). A novel hybrid MPPT for wind energy conversion systems operating under low variations in wind speed. *Energy and Power Engineering*, **12**, 716–728. https://doi.org/10.4236/epe.2020.1212042.

Mokhtari, Y., & Rekioua, D. (2018). High performance of maximum power point tracking using ant colony algorithm in wind turbine. *Renewable Energy*, **126**, 1055–1063. https://doi.org/10.1016/j.renene.2018.03.049.

Mousa, H. H. H., Youssef, A.-R., & Mohamed, E. E. M. (2021). State of the art perturb and observe MPPT algorithms based wind energy conversion systems: A technology review. *International Journal of Electrical Power & Energy Systems*, **126**, 106598. https://doi.org/10.1016/j.ijepes.2020.106598.

Muñoz, E., Ayala, E., & Pozo, N. (2021). Estrategia de Control Fuzzy PI en una Turbina Eólica con Generador de Inducción Doblemente Alimentado para maximizar la Extracción de Potencia en Presencia de Perturbaciones. *Revista Técnica" Energía",* **18**, 1–10. https://doi.org/10.37116/revistaenergia.v17.n2.2021.428.

Muñoz, E., Ayala, E., Pozo, N., & Simani, S. (2020). Fuzzy PID control system analysis for a wind turbine maximum power point tracking using FAST and Matlab Simulink. In *Proceedings of the Brazilian Technology Symposium*(pp. 905–917). Springer. https://doi.org/10.1007/978-3-030-75680-2_100.

Naik, K. A., Gupta, C. P., & Fernandez, E. (2020). Advanced type-2 fuzzy logic–based pitch-angle control strategy for wind energy system. *Wind Engineering*, **44**, 75–92. https://doi.org/10.1177/0309524×19849839.

Nurzaman, I., Harini, B. W., Avianto, N., & Yusivar, F. (2017). Implementation of maximum power point tracking algorithm on wind turbine generator using perturb and observe method. In *Proceedings of the 2017 International Conference on Sustainable Energy Engineering and Application (ICSEEA)* (pp. 45–51). https://doi.org/10.1109/ICSEEA.2017.8267686.

Pande, J., Nasikkar, P., Kotecha, K., & Varadarajan, V., 2021. A review of maximum power point tracking algorithms for wind energy conversion systems. *Journal of Marine Science and Engineering*, **9**, 1187. https://doi.org/10.3390/jmse9111187.

Pathak, G., Singh, B., & Panigrahi, B. K. (2016). Back-propagation algorithm-based controller for autonomous wind–DG microgrid. *IEEE Transactions on Industry Applications*, **52**, 4408–4415. https://doi.org/10.1109/tia.2016.2581144.

Pozo, A., Ayala, E., Simani, S., & Muñoz, E. (2021). Indirect speed control strategy for maximum power point tracking of the DFIG wind turbine system. *Revista Técnica" Energía",* **17**, 92–101. https://doi.org/10.37116/revistaenergia.v17.n2.2021.426.

Reddy, D., & Ramasamy, S. (2019). A back propagation network based MPPT algorithm for grid-tied wind energy system with Vienna rectifier. *International Journal of Renewable Energy Research* **9**, 1097–1107. https://doi.org/10.20508/ijrer.v9i2.9353.g7684.

Rhaili, S. E., Abbou, A., Hichami, N. E., & Marhraoui, S. (2018). A new strategy based neural networks MPPT controller for five-phase PMSG based variable-speed wind turbine. In *Proceedings of the 2018 7th International Conference on Renewable Energy Research and Applications (ICRERA)* (pp. 1038–1043). https://doi.org/10.1109/icrera.2018.8566822.

Sabzevari, S., Karimpour, A., Monfared, M., & Naghibi Sistani, M. B. (2017). MPPT control of wind turbines by direct adaptive fuzzy-PI controller and using ANN-PSO wind speed estimator. *Journal of Renewable and Sustainable Energy*, **9**, 013302. https://doi.org/10.1063/1.4973447.

Saxena, V., Kumar, N., Singh, B., & Panigrahi, B. K. (2020). A voltage support control strategy for grid integrated solar PV system during abnormal grid conditions utilizing interweaved GI. *IEEE Transactions on Industrial Electronics*, **68**, 8149–8157. https://doi.org/10.1109/TIE.2020.3013771.

Saxena, V., Kumar, N., Singh, B., & Panigrahi, B. K. (2021a). A spontaneous control for grid integrated solar photovoltaic energy conversion systems with voltage profile considerations. *IEEE Transactions on Sustainable Energy*, **12**, 2159–2168. https://doi.org/10.1109/tste.2021.3084103.

Saxena, V., Kumar, N., Singh, B., & Panigrahi, B. K. (2021b). A rapid circle centre-line concept-based MPPT algorithm for solar photovoltaic energy conversion systems. *IEEE Transactions on Circuits and Systems I: Regular Papers*, **68**, 940–949. https://doi.org/10.1109/tcsi.2020.3038114.

Semrau, G., Rimkus, S., & Das, T. (2015). Nonlinear systems analysis and control of variable speed wind turbines for multiregime operation. *Journal of Dynamic Systems, Measurement, and Control*, **137**, 041007. https://doi.org/10.1115/1.4028775.

Downloaded from https://academic.oup.com/jcde/article/10/1/108/6912246 by guest on 07 July 2024

Sierra-García, J. E., & Matilde, S. (2020). Performance analysis of a wind turbine pitch neurocontroller with unsupervised learning. *Complexity*, **2020**, 1–15. https://doi.org/10.1155/2020/4681767.

Sierra-García, J. E., & Santos, M. (2021a). Lookup table and neural network hybrid strategy for wind turbine pitch control. *Sustainability*, **13**, 3235. https://doi.org/10.3390/su13063235.

Sierra-García, J. E., & Santos, M. (2021b). Neural networks and reinforcement learning in wind turbine control. *Revista Iberoamericana De Automática e Informática Industrial*, **18**, 327–335. https://doi.org/10.4995/riai.2021.16111.

Sierra-García, J. E., & Santos, M. (2021c). Switched learning adaptive neuro-control strategy. *Neurocomputing*, **452**, 450–464. https://doi.org/10.1016/j.neucom.2019.12.139.

Sierra-Garcia, J. E., & Santos, M. (2022). Deep learning and fuzzy logic to implement a hybrid wind turbine pitch control. *Neural Computing and Applications*, **34**, 10503–10517. https://doi.org/10.1007/s00521-021-06323-w.

Tiwari, R., & Babu, N. R. (2016). Recent developments of control strategies for wind energy conversion system. *Renewable and Sustainable Energy Reviews*, **66**, 268–285. https://doi.org/10.1016/j.rser.2016.08.005.

Tomás-Rodríguez, M., & Santos, M. (2019). Modelling and control of floating offshore wind turbines. *Revista Iberoamericana De Automática e Informática Industrial*, **16**, 381–390. https://doi.org/10.4995/riai.2019.11648.

Yaakoubi, A. E., Asselman, A., Djebli, A., & Aroudam, E. H. (2016). A MPPT strategy based on fuzzy control for a wind energy conversion system. *Procedia Technology*, **22**, 697–704. https://doi.org/10.1016/j.protcy.2016.01.145.

Zhou, Z., Elghali, S. B., Benbouzid, M., Amirat, Y., Elbouchikhi, E., & Feld, G. (2020). Tidal stream turbine control: An active disturbance rejection control approach. *Ocean Engineering*, **202**, 107190. https://doi.org/10.1016/j.oceaneng.2020.107190.

Zouggar, E., Chaouch, S., Abdelhamid, L., & Abdeslam, D. (2021). Real-time implementation of the MPPT control algorithms of a wind energy conversion system by the digital simulator OPAL_RT. *European Journal of Electrical Engineering*, **23**, 45–52. https://doi.org/10.18280/ejee.230106.

Downloaded from https://academic.oup.com/jcde/article/10/1/108/6912246 by guest on 07 July 2024